Novel Dampening Technique for the Reflected Wave in High Strain-Rate Compression Tests

Pedro Afonso Almada Freitas
pedro.a.freitas@tecnico.ulisboa.pt

Instituto Superior Técnico, Universidade de Lisboa, Portugal

December 2021

Abstract

The difference in deformation conditions between the typical mechanical characterization of materials tests and manufacturing processes represents a great limitation in the work developed in this area. Deformation suffered during manufacturing can cause the material to have a very different behaviour to that which is obtained using conventional uniaxial compression tests which occur typically in the quasi-static regimen.Motivated by this lapse, the present work aims for the development, coming from an existantant apparatus and introducing major upgrades to it in order to obtain an universal mechanical apparatus capable of realizing uniaxial compression tests with a wide variety of deformation conditions. From quasi-static to very high strain-rates. The equipment was validated by reproducing results in the bibliography for Aluminium Alloy AA 1050-O and AISI 1045 steel.
Keywords: Uniaxial compression, strain-rate, mechanical characterization of materials, AA1050, AISI 1045

1. Introduction

The understanding of a material's mechanical behaviour is of utmost importance for the project, development and production of any mechanical component. From consumer goods to machine tools, material selection depends heavily on the expected working conditions. As important as knowing these conditions, the engineer needs to understand profoundly de mechanical behaviour of the material in question. This behaviour is easily obtained for quasi-static conditions with the most common uniaxial compression tests, however, during manufacturing and even during everyday use, the conditions of deformation, mainly the strain-rate and temperature vary widely and there is a lack of information in the bibliography on the behaviour of the materials for these conditions. This lack of information is due, in large, to the complexity of developing an apparaus capable of performing such tests in such variable conditions.

Mechanical characterisation of materials can be done through constitutive models which predict mathematically the behaviour, taking into account the different conditions mentioned above. The development of these empirical models is an important requisite to allow the engineer to compute the expected behaviour of any material with any set of conditions desired. Empirical in nature, these models depend highly in experimental results in order to be correctly developed.

The present work aims to further develop an uniaxial compression apparatus present in the Machining and Micro-Manufacturing laboratory (Lab M3) in Instituto Superior Técnico (IST) making it able to perform these types of tests with a wide band of strain-rates. From quasi-static tests to very high strain-rates and also mechanicaly improving the apparatus so that data acquisition and interpretation is made simpler and clearer.

2. Background

2.1. Mechanical behaviour of materials

Stress-strain curves typically yield engineers with the knowledge to select the material and manufacturing process combination which would be the most efficient for any project. In these curves, which are representative of the mechanical behaviour of materials one can distinguish two relevant responses to applied stress. Elastic and plastic behaviour.

2.1.1 Elastic Behaviour

Elastic behaviour can be represented as a linear function known as Hooke's Law:

$$\sigma = E\varepsilon \tag{1}$$

From equation 1 one can infer that the representation of this behaviour in a stress-strain curve is

linear. This deformation is non-permanent and reversible when unloading the material [1].

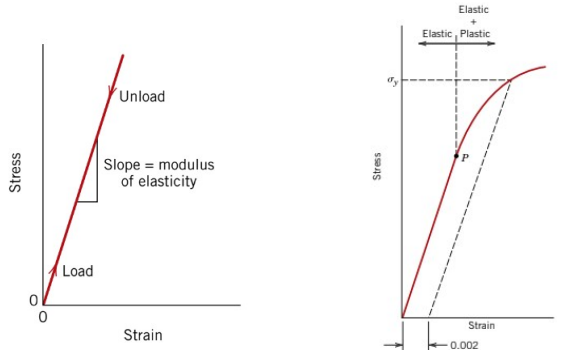

(a) (b)

Figure 1: Elastic deformation in a generic stress-strain curve [1]: (a) Elastic behaviour; (b) Beginning of yielding

As seen on figure 1 (a), Young's Modulus (Modulus of elasticity) is given by the slope of the elastic regime of a stress-strain curve.

When the deformation becomes non-linear there is an onset of permanent, plastic deformation, this is known as yielding.

The yielding point of a material is of utmost importance as it can be considered for most projects that plastic deformation means the catastrophic failure of the component.

The determination of this point is also done through the interpretation of the stress-strain cure. For some materials it is easily pointed out as the point where the deformation becomes non-linear (point P in figure 1 (b)), however for the bulk of materials this point is not easily discernible so a convention was made. The yield point is determined as the intersection of the stress curve with a line parallel to the linear elastic regime, skewed in the strain axis to intercept $\varepsilon = 0.2\%$ of strain. This stress, σ_y is known as the yield stress

2.1.2 Plastic Behaviour

The plastic behaviour is not as easily interpreted and modelled as the elastic behaviour. Many phenomena affect this behaviour which make it increasingly non-linear and difficult to predict, such has strain hardening (2 (a)), or viscous effects.

Temperature (2 (b)) affects the ductility and tenacity of materials usually making them more ductile for higher temperatures. It also has a reologic effect which normally reduces flow stress and creep resistance.

Higher strain-rates, apart from increasing the temperature, have effects on the crystal structure and grain flow of metals [9], these effect typically

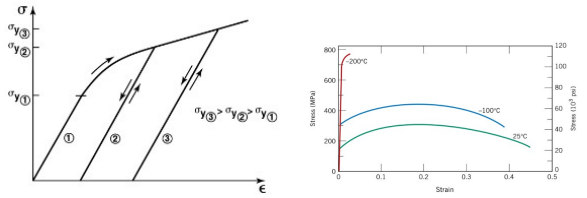

(a) (b)

Figure 2: Plastic behaviour phenomena: (a) Strain-Hardening [5]; (b) Temperature effect on cast iron [1]

produce aa higher flow stress needed for the same strain values. This translates to the stress-strain curve as shown in figure 3

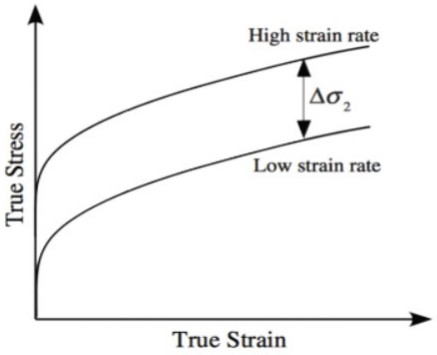

Figure 3: Generic representation of stress-rate effect on stress-strain curves

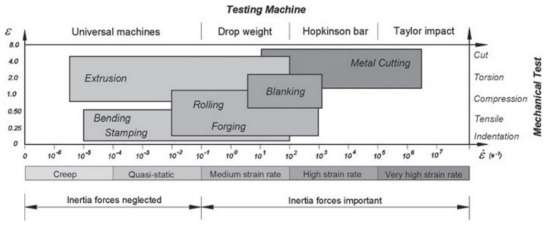

Figure 4: Strain-rate related to manufacturing processes [11]

2.2. Uniaxial compression test

The uniaxial compression test, target of this study, consists essentially of compressing between two compression plates a cylindrical specimen, registering the load applied and the displacement of the plates or the instant height of the sepcimen, as can be seen by the diagram in figure 5.

Having the values for applied force, F, and instant specimen height, h_i one can obtain the stress-strain curve with the following equations:

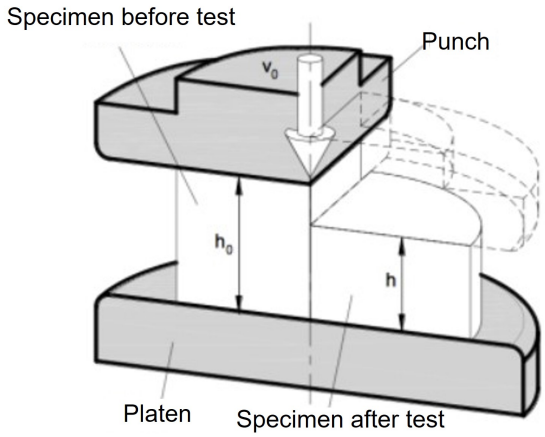

Figure 5: Uniaxial compression test [11]

$$\sigma = \frac{F}{A_i} \tag{2}$$

where A_i is the instant specimen section area, computed with the imcompressibility condition:

$$V_i = V_o \iff A_0 h_0 = A_i h_i \tag{3}$$

$$A_i = \frac{A_0 h_0}{h_i} = \frac{A_0 h_0}{h_0 - \Delta h} \tag{4}$$

The strain, ε, is obtained with the following expression [11]:

$$\varepsilon = -\int_{h_0}^{h_i} \frac{dh}{h} = ln\left(\frac{h_o}{h_i}\right) \tag{5}$$

2.3. Split Hopkinson Pressure Bar

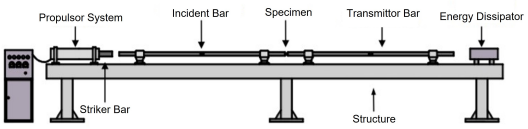

Figure 6: Typical SHPB diagram [6]

The equipment developed in the present work is highly based on the Split Hopkinson Pressure Bar (SHPB). The diagram from figure 6 shows the typical instalation of such an apparatus. The technique consists essentially of exciting the two bars (incident and transmission) above their resonance frequency and studying the behaviour of the propagation waves [3].

The bars should be kept in elastic deformation while providing sufficient energy for the specimen to be plastically deformed, so the material should be chosen carefully.

The incident bar is typically excited with a striker bar. The impact generates an elastic propagation wave which is partly transmitted to the specimen and the transmission bar, and partly reflected. Both these bars are instrumented with extensometers in a Wheatsone bridge and the behaviour of the incident, reflected and transmitted wave is analysed and treated mathematically to obtain stress-strain and strain-rate curves [7]. This procedure, however typically introduces many errors so care should be taken when interpreting results.

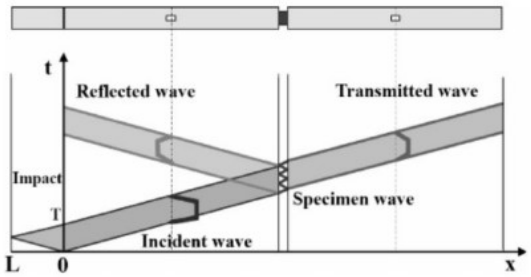

Figure 7: Wave propagation diagram

The diagram in figure 7 easily ilustrates the principle of the Split Hopkinson Pressure Bar.

The elastic waves propagate along the bar at the material's speed of sound:

$$c_b = \sqrt{\frac{E}{\rho}} \tag{6}$$

and the pulse created by the striker bar which generates said waves develops in a time interval dependant of the striker bar's length, L_{st} [12] given by:

$$t_{pulse} = \frac{2L_{st}}{c_{st}} \tag{7}$$

where c_{st} is the speed of sound in the striker bar.

The apparatus in the present work was developed introducing several upgrades to a machine which was already present in the lab and had been developed by several other students, more lately by Saragoça (2021), some of his work is described below.

2.4. Structure

The machine's structure is divided in two, namely the base structure, composed of an I-beam welded to 3 pillars fixed to the floor of the lab in order to form a closed structural ring capable of maintaining rigidity when stressed. The pillars are furthered reinforced with 2 U-beams welded at half-height of said pillars as can be observed in figure 8 (a).

Coupled with this base structure there is a support structure as seen in figure 8 (b). Two zones can be distinguished from this figure, the test zone,

(a) (b)

Figure 8: Structural components [10]: (a) Base Structure; (b) Support Structure

where the specimen is actually compressed and the dissipation zone where the energy given to the bar is dissipated.

These components were fabricated in AISI 1045 with $20mm$ plates. Threaded rods in tension are used to minimise the bending suffered by the C-structures.

The two zones are connected through an I-beam fastened to both plates which are fastened to the top flange of the base structure's I-beam. The first I-beam mentioned is used also for the guiding system of bearings which guides the bars.

2.5. Incident and transmission bar

The incident and transmission bars are fabricated in a Titanium Alloy Ti6Al4V, they are cylindrical with $30mm$ diameter and $500mm$ and $1500mm$ in length, respectively. In the bar ends where the compression of the specimen occurs, compression rods made in Tungsten Carbide were added. These bars are $18mm$ in diameter.

There are two sets of bars used depending on the temperature condition of the test. For room temperature tests, the bars with short rods (Figure 9 (a)) are used. For high temperature tests, the bars with long rods which allow the installation of the electrical oven are used. This second set of bars should be exclusively be used for high temperature tests because as the rods are very slender ($80mm$ in length and only $18mm$ in diameter) they are more susceptible to fracture during operation.

(a) (b)

Figure 9: Bar ends with compression rods: (a) Short Rods; (b) Long Rods

Contrary to the traditional SHPB, where both bars are equipped with extensometers, in this case only the transmission bar is instrumented in order to register the applied load during the test. For the displacement, different types of sensors, which are explained later, are used.

2.6. Momentum dissipator

For the high speed compression tests, the bars are excited with a great amount of momentum which needs to be safely dissipated so as to damage to the apparatus' components and also to try and make the wave captured by the Wheatstone bridge as clear as possible.

A dissipating block composed of $25kg$ of steel was installed on the end of the apparatus so as to absorb the energy of the bar which collides with it at the end of the tests. Hydraulic dampers were also introduced to avoid the rebounding effect ijn the bar after the collision. These systems are presented in figure 10.

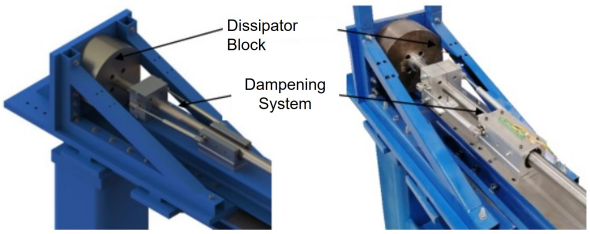

Figure 10: Momentum trap and dampers

2.7. Actuators

Related to the different strain-rates which are the objective of the developments made in the present work, different actuators must be used.

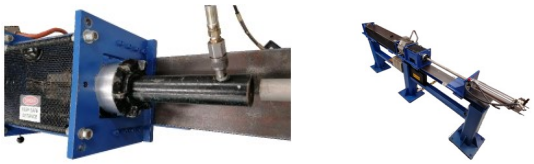

(a) (b)

Figure 11: Different actuators available: (a) Hydraulic actuator; (b) Pneumatic actuator

2.7.1 Hydraulic Actuator

For quasi-static uniaxial compressive tests, the hydraulic actuator (Fig. 11 (a))is used. This actuator was removed from an hydraulic press and is operated using a pedal hydro-pneumatic pump which allows to control the acting speed with a pressure regulator.

2.7.2 Pneumatic Actuator

To obtain high strain-rates, over $1500s^{-1}$ the pneumatic actuator (Fig. 11 (b)) is used. This is es-

sentially a gas gun, with a pressure vessel, a barrel which guides the striker bar until it collides with the incident bar, and a valve which opens and guides the compressed air out of the vessel, through the barrel, accelerating the projectile. As the vessel volume is constant, the energy provided to the bar, neglecting losses due to friction is only dependant on the air pressure. Keeping the pressure and thus the energy constant, the velocity of the striker bar is altered by changing its mass. Therefore, there is a set of projectiles ranging from 250g to 3000g to cover a wide array of velocities.

2.7.3 Electromagnetic Actuator

Having actuators for the quasi-static and high strain-rate tests, there was a gap in the medium strain-rates that needed to be filled. These types of strain-rates can be obtained using the electromagnetic actuator developed by Pinto (2009). This actuator is capable of exciting the incident bar with sufficient energy for the compression test to be performed however, in slow enough speeds so as to obtain strain-rates lower than those obtained with the pneumatic cannon mentioned above.

3. Development

3.1. Moving Actuator Selector

In order to make it possible to use the three types of actuators described above, a moving actuator selector was built, using the old structure on which the electromagnetic gun was stationed, linear bearings and tracks were installed so as to permit the quick and easy actuator selection. This installation is illustrated in figure 12.

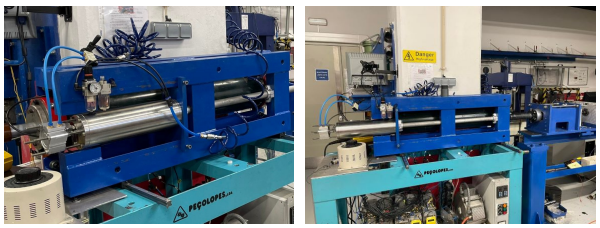

(a) (b)

Figure 12: Moving Actuator Selector: (a) High and medium speed configuration; (b) Quasi-Static configuration

3.2. Dissipation Bar

With the installation of the new actuator selector, a lot of space on the support structure was freed which permitted the installation of a new component to the energy dissipation system, a dissipation bar. The purpose of this was to absorb the energy in the transmitter bar and minimise the wave that was reflected back into the load sensor installed in this bar.

A new, Titanium alloy, $30mm$ diameter and $950mm$ in length bar was then introduced into the system, as well as an extra set of linear bearing to support it and an extra set of hydraulic dampers. To support this new bar, a new, longer support structure I-beam was also manufactured and installed.

For the dissipation bar to perform as intended, a new damping system was developed and installed which consists of having the bars pushed against each other so that, upon impact, the elastic propagation wave is mostly transmitted to the dissipation bar and then takes longer to be reflected back to the transmitter bar. This new system, in comparison to the previously existent is presented in figure 13.

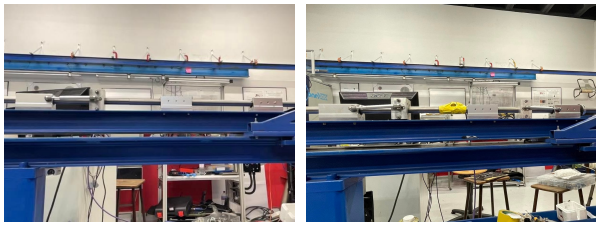

(a) (b)

Figure 13: Transmitter and dissipation bar interface: (a) Old dampening system; (b) Developed dampening system

3.3. Electric Oven

An electric oven is used to get the test zone and specimen into the desired temperature. A commercial oven is used with nominal temperature equal to 1000^{o}C. In previous works this oven was powered using a variable resistance transformer and the test temperature controlled using a pyrometer gun. For the present project the oven's commercial controller was repaired and adapted in order to be compatible with the apparatus to greatly facilitate this process.

Figure 14: Electric Oven and controller

3.4. Data acquisition

In order to obtain results off of the mechanical components mentioned above the apparatus was instrumented with several types of sensors.

The data needed to be acquired in order to obtain a stress-strain curve from a compression test is the applied load and the instant height of the specimen

3.5. Displacement Sensors

Two types of displacement sensors were used depending on the set of bars being used. The inductive sensors for the short rod, room temperature bars and the linear potentiometers for the long rod, high temperature bars.

3.5.1 Inductive Sensors

The inductive sensors, developed by Pedro Santos (2019), are based on the principle of electromagnetic induction between coils. The electric current on one coil generates an electromagnetic field that will induce an electric current on the opposite coil.

This version uses an aluminium coupling instead of two coils however the principle is the same. The distance between plates varies the induced electric current. Based on this concept, and by maintaining a constant voltage in the emitter coil, it is possible to determine the distance between plates through the voltage measured as the output of the coil.

The coil is powered by a signal generator and for the DAQ to read the signal, it needs to be rectified from AC to DC.

The rectifier consists of a bridge of semiconductors insulated in a Zinc box to avoid signal noise as displayed in figure 15.

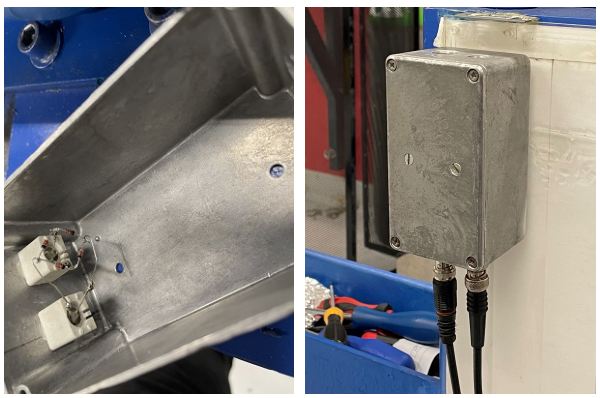

(a) (b)

Figure 15: Signal rectifier: (a) Diode Bridge; (b) Insulating Box

3.5.2 Linear Potentiometers

The electric oven installed in the test area prevents the use of the inductive sensors previously described. An alternative solution was developed using linear sliding potentiometers.

To improve cable management, a data acquisition box, containing the electrical circuitry and tension sources necessary to run the sensors was developed (Fig. 16 (a)). The installation of these sensors on the bars was also improved to prevent damage and improve cable management as mentioned before (Fig. 16 (b)).

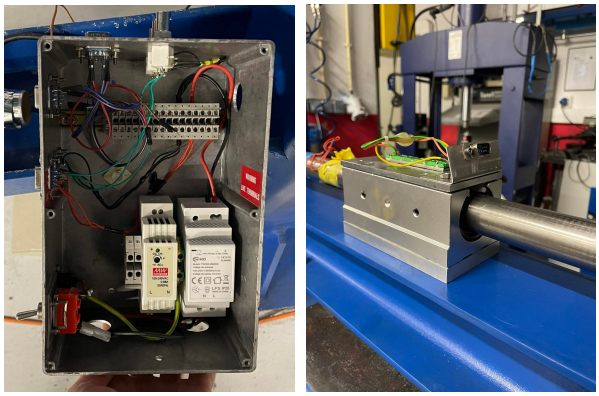

(a) (b)

Figure 16: Data acquisition system: (a) Data acquisition box; (b) Linear potentiometers installatio

3.6. Load Cell

The applied force is registered using a load cell installed in the bars with a Wheatstone bridge of extensometers. The extensometers are extremely sensitive so the circuit is protected with epoxy resin and insulating tape as can be seen on figure 17.

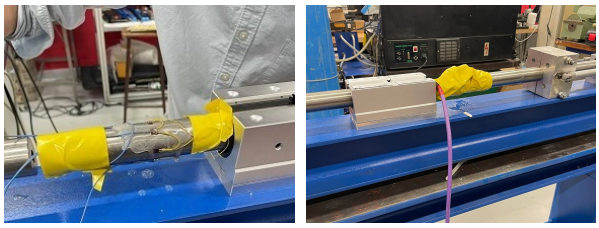

Figure 17: Wheatstone bridge installation

The load cell is excited with a signal amplifier configured with a gain of 500 and $10V$. These load cells are calibrated using a commercial load cell between the compression rods and applying pressure. The signal from both sensors is compared and the calibration curve is obtained.

3.7. Final apparatus

The final result is displayed in figure 18 in its low-speed configuration (a) and high-speed configuration (b)

(a) Quasi-Static tests (b) Dynamic Tests

Figure 18: The complete developed apparatus: (a) Quasi-Static Tests; (b) Dynamic Tests

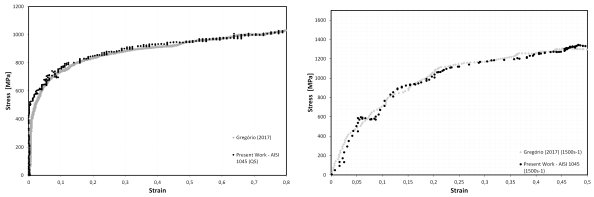

(a) (b)

Figure 20: Stress-strain curves for AISI 1045: (a) Quasi-Static compression test; (b) $\dot{\varepsilon} = 1500s^{-1}$ compression test

4. Results

4.1. Apparatus Validation

In order to asses the validity of the apparatus developed and its results, the author tried to reproduce results documented in the bibliography. Firstly, an Aluminium Alloy 1050-O was used, for which the work developed by Reis (2016) [8] was used as reference for the Quasi-Static tests. For the high strain-rate tests, the work developed by Santos et al. (2017) [2] was used. The specimens were obtained with the same process and subjected to an Annealing heat treatment.

To validate the apparatus in higher strength materials a steel alloy AISI 1045 was used to reproduce the work developed by Gregório (2017). The specimens used were obtained from the same source.

The specimens used in both studies are cylindrical with inital diameter $\phi_0 = 6mm$ and initial height $h_0 \simeq 6,3mm$

In the following figures 19 and 20, in black is the curve obtained in the present work and in gray the references used.

4.1.1 Aluminium Alloy AA1050-O

In figure 19 a good convergence with the bibliography was observed for the AA1050-O.

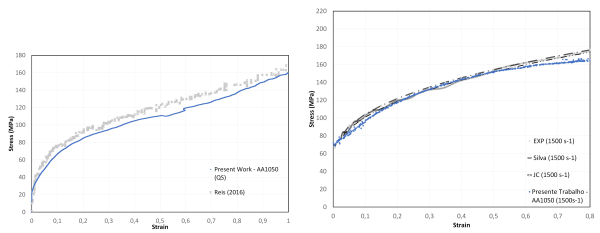

(a) (b)

Figure 19: Stress-strain curves for AA1050-O: (a) Quasi-Static compression test; (b) $\dot{\varepsilon} = 1500s^{-1}$ compression test

4.1.2 Steel AISI 1045

For the AISI 1045 the curves in figure 20 show, again a convergence with the work presented in [4].

These results require some data treatment due to a faulty signature of the captured load cell signal due to noise combined with some difficulties experienced when calibrating the displacement sensors.

4.2. Characterisation of the signal and noise registered

Having observed that the improvements to the signal were not as significant as expected and in order to serve as possible orientation for future upgrades to be implemented in the apparatus, a study of the captured signal and the possible sources of wave distortion was performed.

The data used was acquired during a high strain-rate test of AISI 1045 Steel. Using the $250g$ striker and $8bar$ of air pressure in the vessel These were the conditions chosen due to the velocity and length of the projectile. The shorter stiker bar produces a shorter pulse (from equation (7)), ensuring wave separation thus making the interpretation of the signal possible.

When studying the signal, 5 reflected peaks were observed in the first $1000\mu s$ after impact as shown in figure 21.

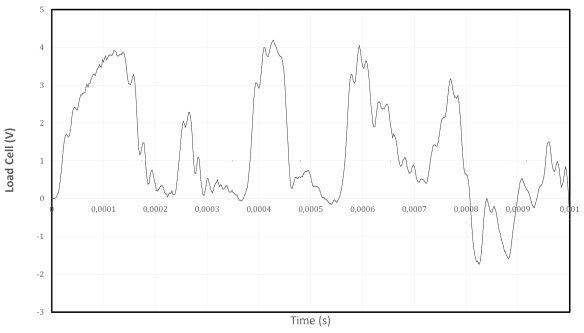

Figure 21: First $1000\mu s$ after impact

To try and understand the origin of these reflections, the diagram shown in figure 22 was developed. The interfaces of the bars were considered as possible reflection points and the Tungsten Carbide compression rods were neglected to facilitate calculations. In the diagram, 5 possible waves in

different time instants are distinguished.

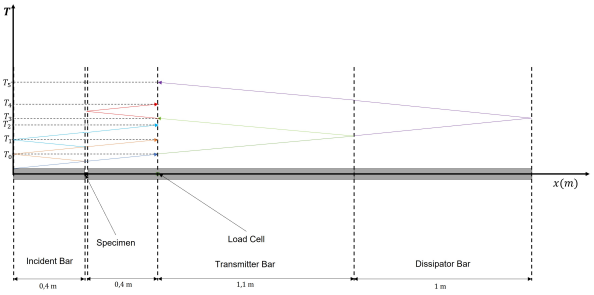

Figure 22: Wave propagation diagram

The speed of sound in the bar was obtained experimentally, studying the signal obtained with the two load cells implemented, knowing the distance between them ($1.1m$) and determining the time interval using the plot in figure 23 ($240\mu s$), the speed of sound was calculated as $c_b = 4583,33$.

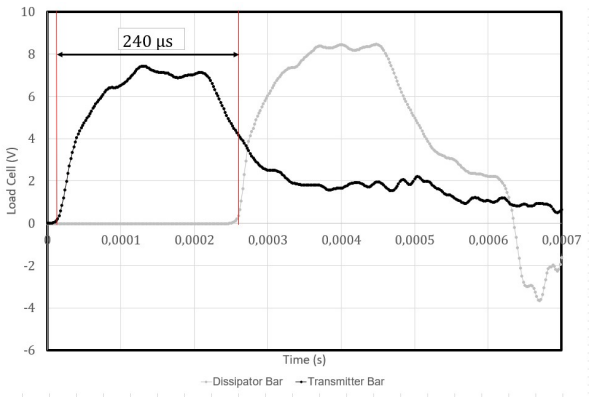

Figure 23: Two load cells signal

From the diagram in 22 the distance travelled by the waves is easily inferred, with the calculation of c_b one can now obtain the time instants after impact for which a reflected wave is expected, as presented in the following table 1:

Waves	Distance (m)	Time (μs)	Time after T_0 (μs)
T_0	0,8	174,55	0
T_1	1,6	349,09	174,55
T_2	2,4	523,64	349,09
T_3	3	654,55	480,00
T_4	3,8	829,09	654,55
T_5	5	1090,91	916,36

Table 1: Expected time calculation

Cross referencing the data on table 1 with the graph on figure 21, the graph presented on figure 24

Considering the expected positions of reflected waves were predicted with a small error of $\approx 50\mu s$ in some cases, this approach was considered to be

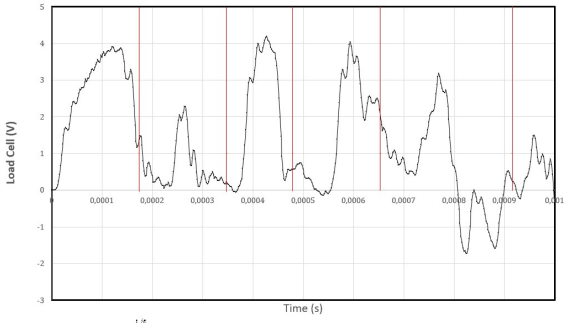

Figure 24: Signal with times from table 1

acceptable for the study on the influence of possible mechanical changes on the system.

4.3. Possible changes

Firstly, the dissipator system developed by the author immediately proves to not work as expected. The bars were expected to behave as if it was one long bar, and the peaks in instants T_3 and T_4, caused by the interface of the bars would not appear.

The diagram highlighting this change is presented in figure 25

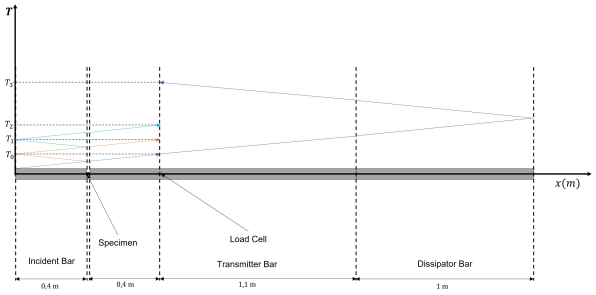

Figure 25: Wave propagation diagram for one long transmission bar

As shown in figure 25 two of the reflected waves (T_3 and T_4) would be expected to be eliminated from the signal. Even though it proves a significant upgrade, the system could be further simplified if the waves pertaining to instants T_1 and T_2 were to appear later.

Introducing a longer incident bar would be key for this to happen. Maintaining the longer transmitter bar and introducing a longer incident bar, the wave propagation diagram turns out as presented in figure 26

Performing the calculations as shown before to determine the expected times, the results were as follows in table 2.

Interpreting the results from the table and comparing with table 1, upgrade is significant. The signal time unaffected by noise would be 3 times as long which means making the possible pulse time

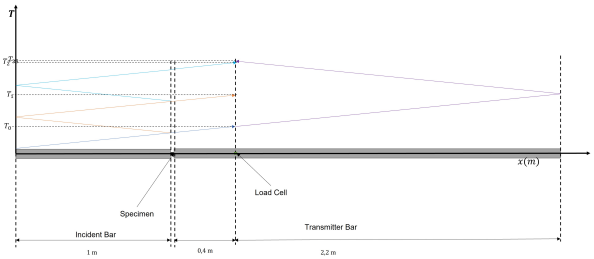

Figure 26: Wave propagation diagram for longer incident and transmitter bars

Waves	Distance (m)	Time (μs)	Time after T_0 (μs)
T_0	1,4	305,45	0
T_1	3,4	741,82	436,36
T_2	5,4	1178,18	872,73
T_3	5,8	1265,46	960,00

Table 2: Expected time calculation for apparatus with longer transmitter and incident bars

without interference 3 times longer as well. This would make the signal obtained for tests with longer striker bars, thus lower strain-rates much more unaffected by noise and their results much clearer and safer.

The effect of changing the load cell's position along the bar was also studied however the results did not show any signs of this being an upgrade, especially when compared with the addition of a longer incident bar so, for brevity, the results will not be shown.

5. Conclusions

The development of the experimental apparatus and posterior successful validation allows one to conclude that the main objective of this work was correctly achieved. The upgrades implemented allow the same apparatus, same sensors and same data acquisition and treatment to be used for uniaxial compression test in a very broad range of strain-rates and temperatures. An apparatus with such conditions is unheard of, and is a great advancement in what is available as of the author's knowledge to this date.

The wave dissipation system developed proved uneffective however, as presented in section 4 the present investigation allowed the study and project of some mechnical upgrades that, in theory, should further upgrade the signal. Looking into some of the solutions presented and implementing them would be a good step in order to explore the full capabilities of this apparatus.

The versatility and ease of operation on a mechanical level are some of the major strong suits of this apparatus. However on a data acquisition level there are still some aspects that could be improved. The apparatus would benefit from more reliable displacement sensors. Also, the calibration procedure for the inductive sensors, using for example linear sensors would be a significative improvement.

Due to time constraints, a wider study of materials' characterisation was not possible. This would be of extreme importance not only to document these results but also to further validate the apparatus' operation and come across possible problems that might have been overlooked by the author.

References

[1] W. Callister and D. Rethwisch. *Materials Science and Engineering: An Introduction, 8th Edition*. Wiley, 2009.

[2] T. dos Santos, J. C. Outeiro, R. Rossi, and P. Rosa. A New Methodology for Evaluation of Mechanical Properties of Materials at Very High Rates of Loading. *Procedia CIRP*, 58:481–486, 2017. 16th CIRP Conference on Modelling of Machining Operations (16th CIRP CMMO).

[3] J. Field, S. Walley, W. Proud, H. Goldrein, and C. Siviour. Review of experimental techniques for high rate deformation and shock studies. *International Journal of Impact Engineering*, 30(7):725–775, 2004. Fifth International Symposium on Impact Engineering.

[4] A. J. d. V. L. Gregório. Ensaios de Impacto e Elevadas Velocidades de Deformação. Master's thesis, Instituto Superior Técnico, 2017.

[5] R. Jones. *Deformation Theory of Plasticity*. Bull Ridge Pub., 2009.

[6] J. M. G. T. Pinto. Avaliação do Comportamento Mecânico de Blindagens Balísticas. Master's thesis, Instituto Superior Técnico, 2009.

[7] K. T. Ramesh. *High Rates and Impact Experiments*. Springer US, Boston, MA, 2008.

[8] A. P. d. Reis. Efeito de Escala na Resistência Mecânica de Materiais. Master's thesis, Instituto Superior Técnico, 2016.

[9] G. T. (Rusty) Gray. High-Strain-Rate Deformation: Mechanical Behavior and Deformation Substructures Induced. *Annual Review of Materials Research*, 42(1):285–303, 2012.

[10] M. E. L. Saragoça. Desenvolvimento de Máquina para Ensaios de Impacto a Alta Velocidade de Deformação e Elevada Temperatura. Master's thesis, Instituto Superior Técnico, 2020.

[11] C. M. A. Silva, P. A. R. Rosa, and P. A. F. Martins. Innovative Testing Machines and Methodologies for the Mechanical Characterization of Materials. *Experimental Techniques*, 40:569–581, 2016.

[12] E.-H. Wong and Y.-W. Mai. 12 - rate-dependent stress–strain properties of solders. In E.-H. Wong and Y.-W. Mai, editors, *Robust Design of Microelectronics Assemblies Against Mechanical Shock, Temperature and Moisture*, Woodhead Publishing Series in Electronic and Optical Materials, pages 411–446. Woodhead Publishing, 2015.